

Stability Analysis of MEMS Devices through Eigenvalues

Advanced Finite Elements – Final Project
Professor - Carlos Felippa

Joe Pajot

Michael Rauli

May 8, 2003

Contents

1	Introduction	3
2	Analytical Models used for MEMS Analysis	3
2.1	The Plate-spring Model	3
2.2	Torsional Plate Model	4
3	Computational Framework for Electro-mechanical Analysis	6
3.1	Modeling of Electro-mechanical Problem	6
3.2	Solution of Coupled Equations	7
4	Solution of Eigenvalue Problem	9
5	Numerical Examples and Analysis of Results	11
5.1	Plate-spring Example	11
5.2	Torsional Plate Example	13
5.3	Cantilever Beam Example	17
6	Conclusions	18

1 Introduction

Electrostatically actuated MEMS devices may exhibit instabilities in their modes of operation. Capacitive devices pull-in and make contact between electrodes due to the strength of the applied electrostatic load. This behavior may be undesirable if the device operates in analog, conversely, it may be wanted if digital responses are required for proper performance.

What we propose to attempt in this project is to characterize the stability of MEMS devices by examining the eigenvalues of the coupled electro-mechanical system. The authors hope that the instability of the system at pull-in will manifest itself in the eigenvalues of the system. Rather than examining all of the thousands of eigenvalues from the coupled system, only the eigenvalue of smallest magnitude will be calculated and studied. Three geometrically distinct problems will be studied: a parallel plate-spring model, a torsional plate model, and a cantilever beam model. The first two of these problems have analytical solutions for their pull-in behavior, which will be paramount in verifying our analyses.

2 Analytical Models used for MEMS Analysis

In this section the theoretical results for two of the geometries examined later are presented. These problems are the plate-spring and the torsional plate problems. These problems are simple enough that they can be adequately modeled as one degree of freedom systems. This geometric simplicity allows one to derive closed form solutions for the pull-in behavior of these devices.

2.1 The Plate-spring Model

Figure 1 contains a visualization of the geometry of the plate-spring model. Two parallel electrode plates of overlap area A are initially set apart a distance d_0 ; the bottom plate is held fixed while the upper plate is held in place by a set of linear springs characterized by their effective elastic restoring stiffness K , such that $f = Kz$. The upper plate is assumed to only displace an amount z in the vertical direction. Finally, a voltage V is assumed between the electrodes.

The applied voltage between the plates creates an electrostatic force

$$F_e = -\frac{1}{2}\epsilon V^2 A \frac{1}{(d_0 - z)^2} \quad (1)$$

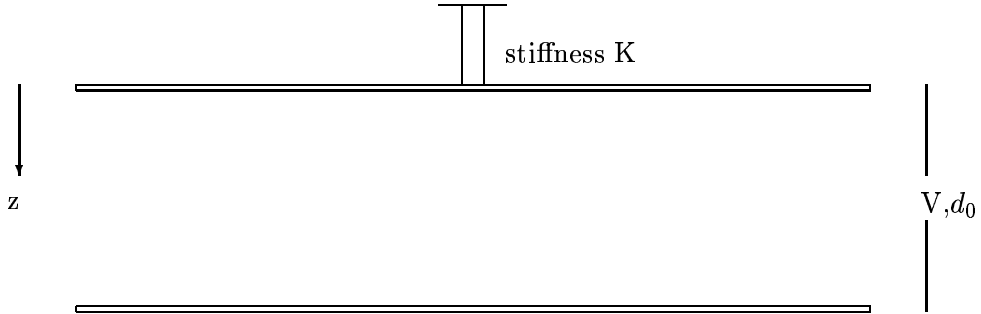


Figure 1: Visualization of Spring-plate Model

where ϵ is the electric permittivity of the material in the gap between the electrodes. Equating the applied electrostatic force (Eq 1) to the elastic restoring force of the spring produces the equilibrium equation solved for the voltage V

$$V = (d_0 - z) \sqrt{\frac{2Kz}{\epsilon A}} \quad (2)$$

Pull-in occurs when the derivative of Eq 2 with respect to z equals zero. Carrying this differentiation out, one can show that

$$\text{Pull-in occurs at } z_{pi} = \frac{d_0}{3} \quad (3)$$

Back substitution of Eq 3 into Eq 2 produces an expression for the theoretical pull-in voltage.

$$\text{Pull-in occurs at } V_{pi} = d_0^{3/2} \sqrt{\frac{8K}{27\epsilon A}} \quad (4)$$

2.2 Torsional Plate Model

The geometry for the torsion plate problem is shown in Figure 2. Note that the diagram extends out of the page a length b . Here the bottom plate is assumed fixed, while the upper plate is allowed to rotate about an axis extending out of the page. Unlike the plate-spring problem, the electrode geometry is not simply represented by a simple area parameter. Instead, the geometry of the problem is defined by the lengths a_1 , a_2 , and a_3 as shown in Figure 2. The plates are assumed to initially lie a distance h apart, and a voltage V is applied between the electrodes.

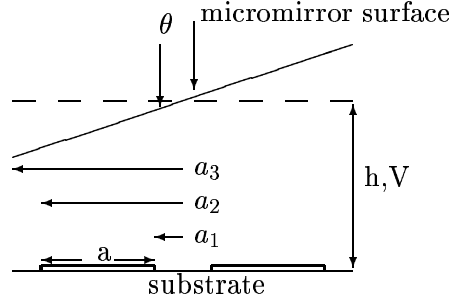


Figure 2: Visualization of Torsional Plate Model

The applied voltage produces an electrostatic torque on the plate. This movement, M , can be expressed as ¹

$$M = \frac{\epsilon V^2 b}{2\theta^2} \left[\frac{h}{h - a_2\theta} - \frac{h}{h - a_1\theta} + \ln \left(\frac{h - a_2\theta}{h - a_1\theta} \right) \right] \quad (5)$$

More insight may be gained by employing the following non-dimensionalization

$$\beta = a_2/a_3 \quad (6)$$

$$\theta_{max} = h/a_3 \quad (7)$$

$$\Theta = \theta/\theta_{max} \quad (8)$$

$$\gamma = a_1/a_3 \quad (9)$$

From these, Eq 5 may be re-expressed as

$$M = \frac{\epsilon V^2 b}{2\theta_{max}^2} \frac{1}{\Theta^2} \left[\frac{1}{1 - \beta\Theta} - \frac{1}{1 - \gamma\Theta} + \ln \left(\frac{1 - \beta\Theta}{1 - \gamma\Theta} \right) \right] \quad (10)$$

Equation 10 clearly shows that the electrostatic moment is primarily governed by the non-dimensionalized geometrical quantities β and γ .

Similar to the plate-spring problem, the assembly discussed thus far is held in place by a set of torsional micro-beams which provide an elastic restoring force K , such that $M_{elas} = K\theta$. Summing the applied and restoring forces to attain equilibrium and solving for the voltage provides

$$V = \left[\frac{2K\theta_{max}^3}{\epsilon b} \right]^{1/2} \left\{ \frac{\Theta^3}{\frac{1}{1-\beta\Theta} - \frac{1}{1-\gamma\Theta} + \ln \left[\frac{1-\beta\Theta}{1-\gamma\Theta} \right]} \right\}^{1/2} \quad (11)$$

¹This derivation is based off the work in Degani *et. al.* [1]

Differentiation of Equation 11 with respect to Θ provides the equation for the pull-in angle Θ_0

$$\frac{3}{1 - \beta\Theta_0} - \frac{3}{1 - \gamma\Theta_0} - \frac{\beta^2\Theta_0^2}{(1 - \beta\Theta_0)^2} + \frac{\gamma^2\Theta_0^2}{(1 - \gamma\Theta_0)^2} + 3 \ln \left(\frac{1 - \beta\Theta_0}{1 - \gamma\Theta_0} \right) = 0 \quad (12)$$

A quick glance at Equation 12 shows that the driving voltage is a highly non-linear function of the desired rotation angle and is strictly a function of the electrode geometry. Analytical solutions only exist if $\gamma = 0$, which is the case of the electrode centered under the rotation axis of the upper plate. In this case the solution to Eq 12 must satisfy

$$\beta\Theta_0 = 0.4404 \quad (13)$$

Utilizing Equation 13, the pull-in angle for a design which has a substrate electrode that is equal to the size of the micro-mirror itself has a theoretical value of approximately 44% of the maximum angle allowed by the gap size. It is also worth noting that if β drops below the value of 0.4404, the pull-in phenomena no longer occurs as the normalized pull-in angle must be greater than one – a non-physical solution. Substitution of Eq 13 into the voltage expression of Eq 11 produces the expression for the torsional plate pull-in voltage

$$V_0 = \left[\frac{K\theta_{max}^3}{\epsilon b} \right]^{1/2} \frac{0.585093}{\beta^{3/2}} \quad (14)$$

3 Computational Framework for Electro-mechanical Analysis

3.1 Modeling of Electro-mechanical Problem

Though only two physical domains are simulated in electro-mechanical analysis, the overall simulation is modeled as a three-field problem. The extra field is a result of the dependence of the electrostatic computational domain on the structural shape. If the structure changes shape due to deformation, this infringes upon the electrostatic domain, thus introducing a non-physical field: the mesh-motion of the electrostatic domain, as is done in aero-elasticity by, for example, Farhat *et. al.* [2].

The following three fields represent the global system and the dependencies of each individual field.

$$S(\mathbf{u}, \mathbf{v}, \mathbf{x}) = 0 \quad \textit{Structure} \quad (15)$$

$$E(\mathbf{v}, \mathbf{x}) = 0 \quad \textit{Electrostatic} \quad (16)$$

$$R(\mathbf{u}, \mathbf{x}) = 0 \quad \textit{Electrostatic mesh} \quad (17)$$

with \mathbf{u}, \mathbf{v} the structural and electrostatic states, respectively and \mathbf{x} being electrostatic mesh displacements.

The above fields (15 - 17) are represented by the following state equations:

$$S = \mathbf{K}\mathbf{u} - \mathbf{f}(\mathbf{v}, \mathbf{x}) \quad (18)$$

$$E = \mathbf{P}\mathbf{v} - \mathbf{g} \quad \text{with } \mathbf{v} \text{ prescribed on } \Gamma^v \quad (19)$$

$$R = \tilde{\mathbf{K}}\mathbf{x} - \mathbf{h} \quad \text{with } \mathbf{x} = \mathbf{u} \text{ on } \Gamma^{E/S} \quad (20)$$

with \mathbf{K} and \mathbf{P} being the stiffness and permittivity matrices, respectively, in a standard finite element representation. The structural load due to mechanical and electrostatic forces is represented by \mathbf{f} . The matrix $\tilde{\mathbf{K}}$ represents the fictitious stiffness of the electrostatic mesh. The vectors \mathbf{g} and \mathbf{h} are generally zero, as E and R are non-zero Dirichlet boundary condition problems, but are inserted here for completeness.

3.2 Solution of Coupled Equations

The structural and electrostatic problems are solved using the finite element method, as mentioned above. The electrostatic problem is solved using non-zero Dirichlet boundary conditions (constrained voltages) in addition to any Neumann boundary conditions, thus obtaining the full voltage state, \mathbf{v} . The electrostatic forces are then determined in the following manner, as outlined by Kaltenbacher *et. al.* [4]. Maxwell's electrostatic stress tensor along the structural-electrostatic interface ($\Gamma^{E/S}$) is computed in each electrostatic interface element, assuming the structure to be a perfect conductor:

$$\mathbf{T}_e = \varepsilon \begin{bmatrix} e_x^2 - \frac{1}{2}\|\mathbf{e}\|_2^2 & e_x e_y & e_x e_z \\ e_x e_y & e_y^2 - \frac{1}{2}\|\mathbf{e}\|_2^2 & e_y e_z \\ e_x e_z & e_y e_z & e_z^2 - \frac{1}{2}\|\mathbf{e}\|_2^2 \end{bmatrix} \quad (21)$$

where ε is the electric permittivity of free space and $\mathbf{e} = [e_x \ e_y \ e_z]$, is the electric field. The electric field, which is the gradients of the voltage, is computed as follows:

$$\mathbf{e} = \int_{\Omega} \mathbf{B}\mathbf{v} \, d\Omega \quad (22)$$

where \mathbf{B} is the “strain-displacement” matrix of finite element analysis. The electric field and voltages have the same differential relationship as do strains and displacements in elasticity. Now, using the formed Maxwell stress tensor (\mathbf{T}_e), the electrostatic interface forces are computed as:

$$\mathbf{f}_e = \int_{\Gamma^{E/S}} \mathbf{T}_e \mathbf{n} \, d\Gamma \quad (23)$$

where \mathbf{n} is the outward normal on $\Gamma^{E/S}$. This is performed on an element level such that:

$$\mathbf{f}_e = \sum_{k=1}^{n_i} \mathbf{f}_k^{(e)} \quad (24)$$

where n_i is the number of elements on $\Gamma^{E/S}$ and the superscript e in parentheses denotes \mathbf{f} for a given element.

The electrostatic forces provide the forcing term for the structural finite element equations, which are solved directly for linear analysis and with a Newton-type method for non-linear analysis, producing \mathbf{u} . The structural displacements on $\Gamma^{E/S}$ prescribe the motion of the electrostatic mesh on $\Gamma^{E/S}$, and the deformations of non-interface nodes are determined using an elasticity finite element model to represent the “stiffness” of the mesh. The prescribed displacements are used as boundary conditions for the finite element problem, and a non-zero Dirichlet boundary condition problem is solved.

The overall coupled system is solved using the staggered procedure of Maute *et. al.* [5], which allows the different analysis techniques, discussed above, to be used independently. An outline of a step, (i), in the staggered procedure proceeds as follows:

1. Determine the electrostatic forces, $\mathbf{f}_e^{(i)}$ with equations 19 and 21 - 24.
2. Compute

$$\mathbf{f}_{e_T}^{(i)} = \mathbf{T}_f \mathbf{f}_e^{(i)} \quad (25)$$

where \mathbf{T}_f is a transformation matrix that accounts for potentially non-matching nodes between sub-domains and is based on the conservative load transfer algorithm of Farhat *et. al.* [3].

3. Compute

$$\mathbf{u}^{(i+1)} = (1 - \theta)\mathbf{u}^{(i)} + \theta\tilde{\mathbf{u}} \quad (26)$$

where $\tilde{\mathbf{u}}$ is the solution of equation 18, solved for \mathbf{u} and θ is an under-relaxation factor $\in [0.5, 0.9]$. This factor is determined in such a way

that the solution of an aero-elastic system is numerically stable. Since in an electro-mechanical system, both fields are elliptic (a fluid is hyperbolic), a better method for computing θ could potentially be determined. Once $\mathbf{u}^{(i+1)}$ is calculated, check the convergence of the solution by comparing $\mathbf{u}^{(i+1)}$ to $\mathbf{u}^{(i)}$. If converged, exit the loop, else, continue to the next step.

4. Transfer $\mathbf{u}^{(i+1)}$ to the electrostatic mesh as in step 2:

$$\mathbf{u}_{\mathbf{T}}^{(i+1)} = \mathbf{T}_{\mathbf{u}} \mathbf{u}^{(i+1)} \quad (27)$$

where $\mathbf{T}_{\mathbf{u}}$ is the same transformation matrix as $\mathbf{T}_{\mathbf{f}}$.

5. Solve equation 20, the mesh-motion, thus determining a new electrostatic mesh configuration. Return to step 1.

4 Solution of Eigenvalue Problem

The electro-mechanical model employed is non-linear, even though equations (18) - (20) are linear. In order to perform an eigenvalue analysis, the system needs to be linearized. There are two configurations around which the system could be analyzed:

1. The configuration after analysis of the system. This is expected to be the better option for accuracy. The drawback to this option is that it is unable to be used in the event that pull-in actually occurs. If pull-in occurs, the electrostatic mesh will become so distorted that the electrostatic elements will invert, resulting in negative Jacobians. The analysis software will exit upon this occurrence. Therefore, eigenvalues can only be obtained before pull-in occurs.
2. The initial configuration. The attractive aspect of this formulation is the fact that eigenvalues can be obtained for voltages exceeding the pull-in voltage because an electro-mechanical analysis is not performed.

As part of this project, results from both linearized configurations will be compared.

The non-linear electro-mechanical system (\mathcal{M}) is linearized about point \mathbf{y}_0 with a Taylor expansion:

$$\mathcal{M} \approx \mathcal{M}(\mathbf{y}_0) + \nabla \mathcal{M}(\mathbf{y}_0) \quad (28)$$

where $\nabla \mathcal{M}(\mathbf{y}_0)$ represents the electro-mechanical Jacobian matrix. As stated by equations (15) - (17), $\mathcal{M}(\mathbf{y}) = 0$, therefore

$$\mathcal{M} \approx \nabla \mathcal{M}(\mathbf{y}_0) \quad (29)$$

The Jacobian matrix (\mathcal{A}) for this electro-mechanical problem appears as follows:

$$\nabla \mathcal{M}(\mathbf{y}_0) = \underbrace{\begin{bmatrix} \frac{\partial S}{\partial \mathbf{u}} & \frac{\partial S}{\partial \mathbf{v}} & \frac{\partial S}{\partial \mathbf{x}} \\ \frac{\partial E}{\partial \mathbf{u}} & \frac{\partial E}{\partial \mathbf{v}} & \frac{\partial E}{\partial \mathbf{x}} \\ \frac{\partial R}{\partial \mathbf{u}} & \frac{\partial R}{\partial \mathbf{v}} & \frac{\partial R}{\partial \mathbf{x}} \end{bmatrix}}_{\mathcal{A}} \quad (30)$$

Evaluating certain terms in \mathcal{A} yields:

$$\mathcal{A} = \begin{bmatrix} \mathbf{K}_{\Omega\Omega} & \frac{\partial S}{\partial \mathbf{v}} & \frac{\partial S}{\partial \mathbf{x}} \\ 0 & \mathbf{P}_{\Omega\Omega} & \frac{\partial E}{\partial \mathbf{x}} \\ \tilde{\mathbf{K}}_{\Omega\Gamma^{E/S}} & 0 & \tilde{\mathbf{K}}_{\Omega\Omega} \end{bmatrix} \quad (31)$$

Where $\tilde{\mathbf{K}}_{\Omega\Gamma^{E/S}}$ is the portion of the fictitious mesh stiffness that couples the interior of the mesh (Ω) to the boundary with the structure ($\Gamma^{E/S}$). The three block diagonal terms are interior matrices.

The ‘(0)’ terms in \mathcal{A} indicate that there is no direct dependence, therefore a partial derivative will evaluate to zero, for example, the term $\partial E / \partial \mathbf{u}$. Though the electrostatic system (E) clearly depends on the structural displacement (\mathbf{u}), the electro-mechanical model does not contain a direct dependence. The mesh displacements (\mathbf{x}) are directly dependent on the structural displacements. The electrostatic field is in turn dependent on the mesh motion, but this would only be captured by a total derivative, not a partial.

The methodology for predicting the stability of the electro-mechanical system will be to look at the eigenvalue of \mathcal{A} with the smallest absolute value (λ_0), with the assumption that the pull-in instability can be predicted by λ_0 . The eigenvalue λ_0 will be obtained through the inverse power method, which returns the lowest absolute value eigenvalue of a matrix. The steps in the inverse power method will be highlighted in order to illustrate some implementation difficulties for the presented electro-mechanical model.

For a given step, (k), the inverse power method proceeds as follows:

Step 0: Initialize $\mathbf{q}^{(k=0)}$, any random vector will work.

Step 1: Compute $\mathbf{z}^{(k+1)} = \mathcal{A}^{-1}\mathbf{q}^{(k)}$.

Step 2: Compute $\lambda^{(k)} = \mathbf{q}^{(k)t} \mathcal{A}^{-1}\mathbf{q}^{(k)} = \mathbf{q}^{(k)t} \mathbf{z}^{(k+1)}$

Step 3: Check convergence of $\lambda^{(k)}$. If converged, exit, if not, continue.

Step 4: Compute $\mathbf{q}^{(k+1)} = \frac{\mathbf{z}^{(k+1)}}{\|\mathbf{z}^{(k+1)}\|}$. Increment k , return to step 1.

The difficulties with the inverse power steps will be highlighted below:

Step 0: No problem

Step 1: The first difficulty arises in the Jacobian matrix, \mathcal{A} , as three off-diagonal block matrices still need to be evaluated. The derivatives $\partial S/\partial \mathbf{v}$, $\partial S/\partial \mathbf{x}$ and $\partial E/\partial \mathbf{x}$ are programmed by hand, taking analytical derivatives of the finite element governing equations. The implementation of this is very lengthy.

In addition to \mathcal{A} being difficult to compute, it is never explicitly formed, as it exists over three different pieces of software. The solution to $\mathcal{A}^{-1}\mathbf{q}^{(k)}$ is computed by a Gauss-Seidel iterative procedure, outlined by Maute *et. al.* [6].

Steps 1 - 4 Since \mathcal{A} exists in three different pieces of software, so do \mathbf{q} , \mathbf{z} and λ . Communication routines need to transmit information between software in order to compute these terms.

5 Numerical Examples and Analysis of Results

5.1 Plate-spring Example

In order to compare computational results to analytical results, the plate-spring model of section 2 was recreated. Figure 3 shows the coarse computational mesh for this problem. The four springs can be seen at the corners of the plate, which is represented by the black triangular elements. The solid grey part of the mesh represents the electrostatic field. The orange markers indicate the presence of applied voltage. The analytical and computational results agree well as the plate reaches pull-in at almost exactly $d_0/3$ in the computational model. This is the value predicted by the analytical model.

The pull-in voltage occurs for the computational problem at 272.74 volts. The eigenvalue computation is carried out for several different applied voltages, in order to study the behavior of the lowest eigenvalue. The behavior

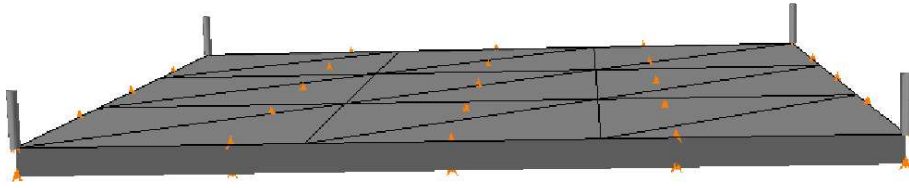


Figure 3: Plate-spring electro-mechanical computational mesh

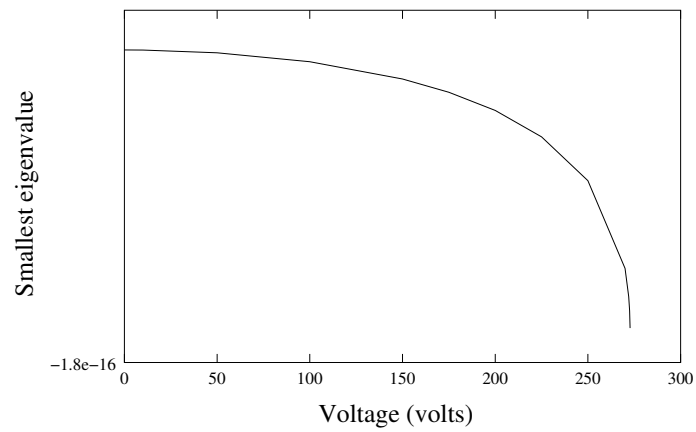


Figure 4: Linearization about analyzed configuration - plate-spring

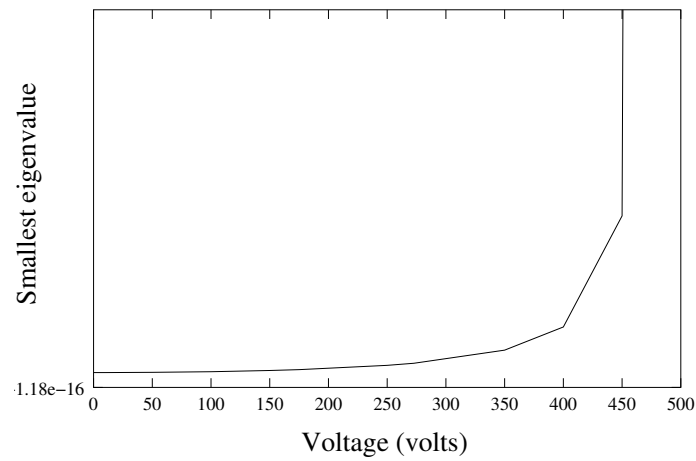


Figure 5: Linearization about initial configuration - plate-spring

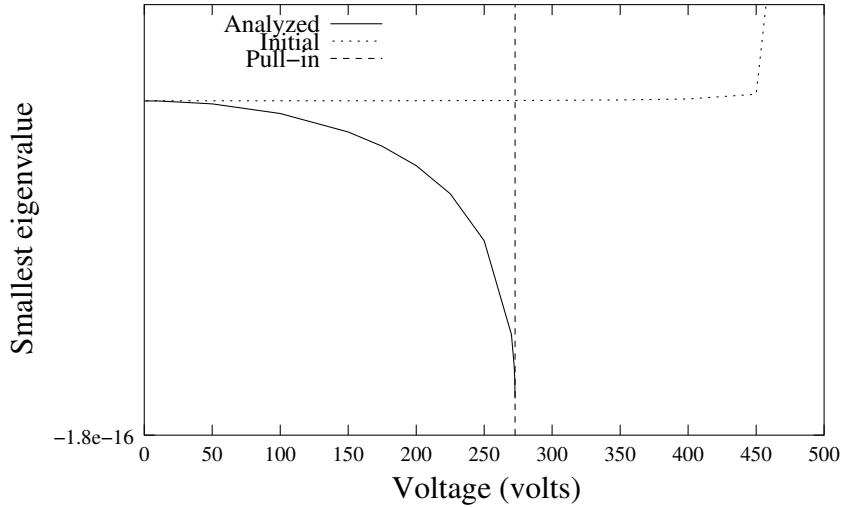


Figure 6: Comparison of linearizations - plate-spring

for the analyzed configuration and the initial configuration is presented in figures 4 and 5, respectively. Figure 6 compares the two results.

When taken separately, the results from linearization about the analyzed and initial configurations both look plausible. However, when viewed together (figure 6), it is clear that the sharp drop in λ_0 far overshoots the actual pull-in voltage. Additionally, the trends are completely opposite. The actual value of the eigenvalues are very small, this is due to the numbers involved in the electrostatic problem. The electrostatic permittivity is $8.85e-12$, rendering the scale of the eigenvalues very small as well.

The hope was that the actual *value* of the eigenvalue would give some indication of the stability when taken by itself. Unfortunately, since the eigenvalue does not equal any number of significance at pull-in, the trend of the eigenvalue remains the most important indicator of stability. Further examples will be looked at in order to shed more light on the problem.

5.2 Torsional Plate Example

A second example studied was that of a torsional plate. The plate is supported by two beams, with six degrees of freedom per node, at its center. The idea was to study the beam with two different modes of instability: rotational and deformational, and see how the eigenvalues behaved for each instability. The different instability modes are triggered by changing the size of the electrode beneath the plate, as was discussed in section 2. If the

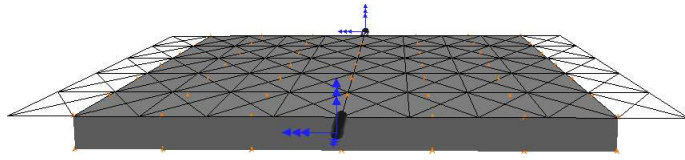


Figure 7: Computational mesh for rotational instability

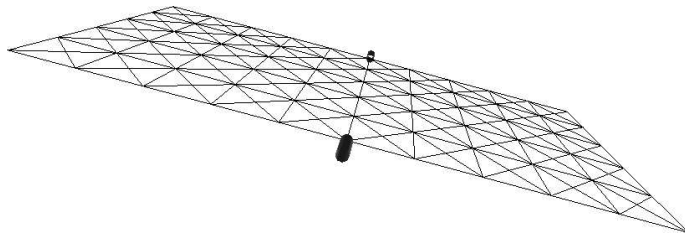


Figure 8: Rotational instability mode - structure

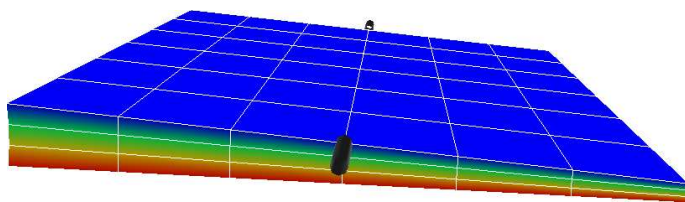


Figure 9: Rotational instability mode - electrostatic

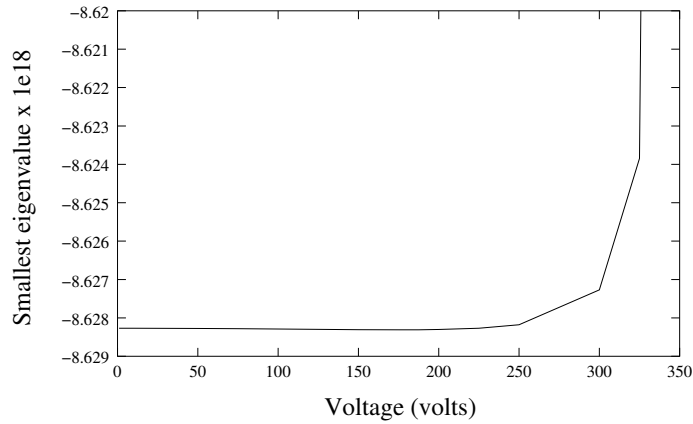


Figure 10: Rotational instability eigenvalues - torsional plate

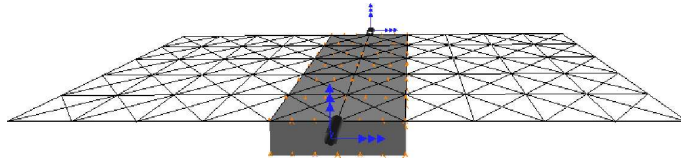


Figure 11: Computational mesh for deformational instability

electrode is made to be thin enough, the beam will pull-in due to its deformation. However, a sufficiently wide electrode will produce enough moment about the beam supports to cause pull-in to occur rotationally. In order to achieve some initial movement in one rotational direction, a slight voltage offset was induced.

The first instability mode studied was the rotational mode. See figure 7 for the computational mesh used. Also, figures 8 and 9 illustrate the pull-in mode for this configuration. The shading in figure 9 is the voltage field. The pull-in voltage was approximately 350 volts. As in the plate-spring model, the trend in the eigenvalues was once again indicative of the stability of the system, but the actual value lacked any real significance. See figure 10 for a plot of the eigenvalues.

The deformational instability of the torsional plate was studied with the mesh in figure 11. Figures 12 and 13 illustrate the instability behavior for the structure and electrostatic, respectively. The shading in figure 13 is the electrostatic forces. In studying the eigenvalues of the deformational instability, it became clear that the actual value of the eigenvalue does have significance. The trend was similar, but opposite, and the eigenvalues were

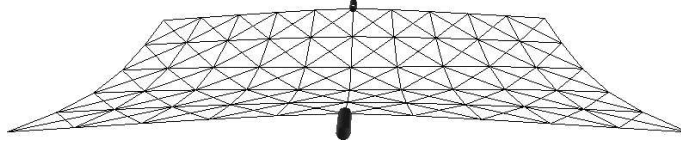


Figure 12: Deformational instability mode - structure

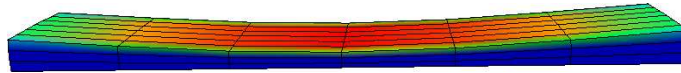


Figure 13: Deformational instability mode - electrostatic

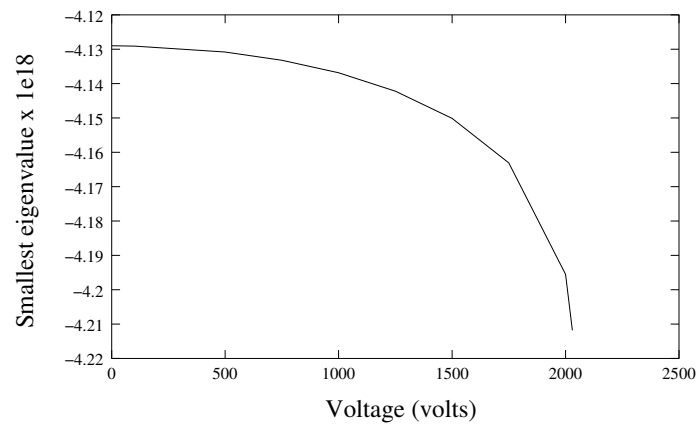


Figure 14: Deformational instability eigenvalues - torsional plate

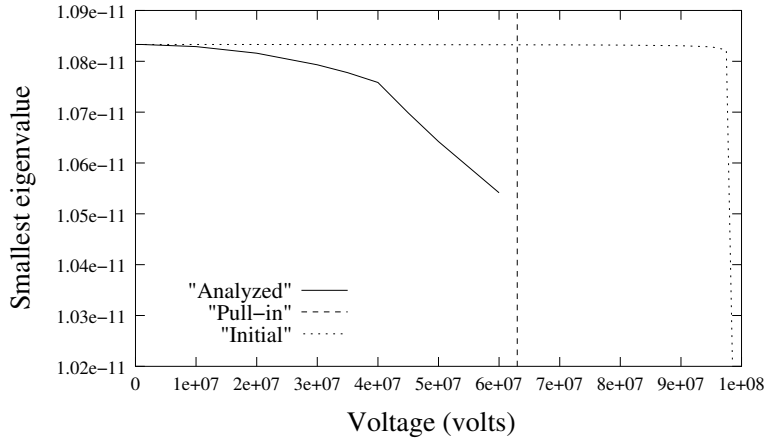


Figure 15: Instability eigenvalues - cantilever beam

different. This suggests that the value is meaningful in itself. See figure 14 for a plot of the deformational eigenvalues.

5.3 Cantilever Beam Example

The final example presented is that of a cantilever beam. The results for this study were similar to the other, more simple structures. The trend in eigenvalues, however is less dramatic. Figure 15 shows results from linearization about the analyzed and initial configurations. The voltage values are so high because this problem was run on a large scale, rather than a micron scale, therefore a rather large voltage value is required for pull-in to occur. This plot further confirms that the initial configuration is very unconservative in regards to predicting pull-in. The interesting note is that the eigenvalues do not drop dramatically at pull-in as they do for the other systems. This is possibly related to the fact that this is a more complicated system than the plate-spring and torsional plate models.

The other notable result from this study is the associated computational times for determining the smallest eigenvalue. It should be noted that the total number of degrees of freedom for this electro-mechanical system is 1,920. As the system approaches instability, the computational time dramatically increases, as illustrated in figure 16 for linearization about the analyzed configuration. This is for two reasons:

1. The inverse power method takes significantly more iterations to converge.

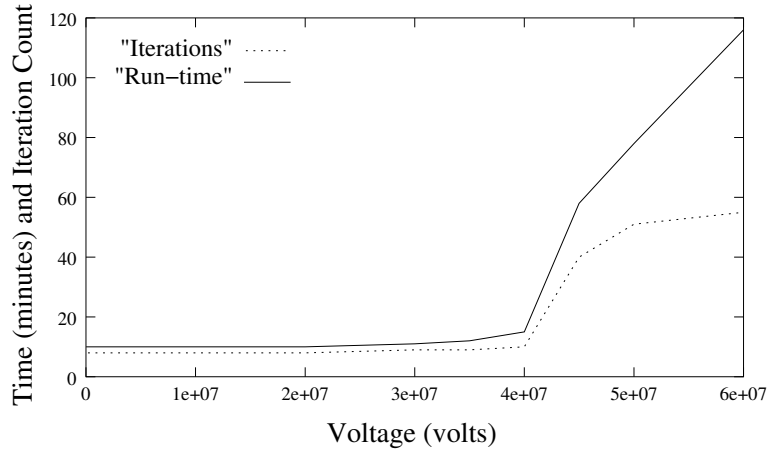


Figure 16: Run-time and iteration count for analyzed configuration - cantilever beam

2. The Gauss-Seidel iterative inversion also becomes much less efficient.

The overall result is a very large computational cost for computing one eigenvalue close to pull-in.

6 Conclusions

At this point in time, the results of this study are hardly conclusive. The eigenvalue plots linearized about the deformed configurations (Figures 4, 10, 14, and 15) show similar characteristic profiles, but no definite statement may be made about the eigenvalue behavior as pull-in is approached. Some eigenvalues are positive while others are negative, and some seem to asymptotically approach infinity as the system nears pull-in while some seem to approach negative infinity. The one behavior that appears consistently throughout the plots is the significant change of the eigenvalues in the voltage region before pull-in. It would be insightful to be able to examine the eigenvalues after pull-in, however the mesh collapse that accompanies pull-in makes this beyond the current capability of the software.

Although the analysis presented in this document lead to no definite conclusions, the authors intend to keep this problem in the scope of their current research work. One thing could definitely lead to more insight into the problem would be to determine a physical interpretation of the computed eigenvalues – assuming that the eigenvalues even have a physical

interpretation. The ability to somehow detect the onset of pull-in without having to trigger one could have a significant impact on the optimization and corresponding sensitivity analyses of MEMS devices. Potentially, the pull-in behavior of a device could be manipulated through the optimization process, increasing the performance of a given MEMS design.

References

- [1] O. Degani, E. Socher, A. Lipson, T. Leitner, D. Setter, S. Kaldor, and Y. Nemirovsky. Pull-in study of an electrostatic torsion micro-actuator. *Journal of Microelectromechanical Systems*, 7(4):373-379, 1998.
- [2] C. Farhat, C. Degand, B. Koobus, and M. Lesoinne. Torsional springs for two-dimensional dynamic unstructured fluid meshes. *Computer Methods in Applied Mechanics and Engineering*, 163:231-245, 1998.
- [3] C. Farhat, M. Lesoinne, and P. LeTallec. Load and motion transfer algorithms for fluid/structure interaction problems with non-matching discrete interfaces: Momentum and energy conservation, optimal discretization and application to aeroelasticity. *Computer Methods in Applied Mechanics and Engineering*, 157:95-114, 1998.
- [4] M. Kaltenbacher, S. Reitzinger, and J. Schoeberl. Algebraic multigrid method for solving 3D nonlinear electrostatic and magnetostatic field problems. *IEEE Transactions on Magnetics*, 36:1561-1564, 2000.
- [5] K. Maute, M. Lesoinne, and C. Farhat. Optimization of aeroelastic systems using coupled analytical sensitivities. In *AIAA 2000-0560, 38th Aerospace Science Meeting and Exhibit, January 10-13, 2000, Reno, NV*, 2000.
- [6] K. Maute, M. Nikbay, and C. Farhat. Coupled analytical sensitivity analysis and optimization of three-dimensional nonlinear aeroelastic systems. *AIAA Journal*, 39(11):2051-2061, 2001.